Hot Spots and Waves in $Bi_2Sr_2CaCu_2O_8$ Intrinsic Josephson Junction Stacks: A Study by Low Temperature Scanning Laser Microscopy

H. B. Wang,[1] S. Guénon,[2] J. Yuan,[1] A. Iishi,[1] S. Arisawa,[1] T. Hatano,[1] T. Yamashita,[1] D. Koelle,[2] and R. Kleiner[2]

[1]*National Institute for Materials Science, Tsukuba 3050047, Japan*

[2]*Physikalisches Institut – Experimentalphysik II and Center for Collective Quantum Phenomena, Universität Tübingen, Auf der Morgenstelle 14, D-72076 Tübingen, Germany*

(Received 3 July 2008; published 9 January 2009)

Recently, it has been shown that large stacks of intrinsic Josephson junctions in $Bi_2Sr_2CaCu_2O_8$ emit synchronous THz radiation, the synchronization presumably triggered by a cavity resonance. To investigate this effect we use low temperature scanning laser microscopy to image electric field distributions. We verify the appearance of cavity modes at low bias and in the high input-power regime we find that standing-wave patterns are created through interactions with a hot spot, possibly pointing to a new mode of generating synchronized radiation in intrinsic Josephson junction stacks.

DOI: 10.1103/PhysRevLett.102.017006 PACS numbers: 74.50.+r, 74.72.Hs, 85.25.Cp

Terahertz (THz) physics and technology still lacks good active devices (e.g., for nondestructive materials diagnostics or chemical and biological sensing), a problem often referred to as the "Terahertz gap" [1]. When a dc voltage V is applied to a Josephson junction the supercurrent oscillates at a frequency $f = V/\Phi_0$, where $\Phi_0 \approx 1$ mV/484 GHz is the flux quantum. Unfortunately, f is limited by the superconducting energy gap, restricting operation of conventional junctions to $f < 700$ GHz or so. Further, a single junction produces a small output power in the pW to nW range. Cuprate superconductors, having higher energy gaps, at least in principle allow to operate Josephson devices up to the THz regime, although many junction types have a strong internal damping, again restricting their usability to the sub-THz regime. The exception is a stack of intrinsic Josephson junctions that are naturally formed by the crystal structure, e.g., in $Bi_2Sr_2CaCu_2O_8$ (BSCCO) [2,3].

High-frequency emission of unsynchronized intrinsic junctions has been observed up to 0.5 THz [4]. Various strategies to achieve synchronized THz radiation included the use of shunting elements in parallel to small sized stacks [5–7], the excitation of Josephson plasma oscillations via heavy quasiparticle injection [8,9] or the investigation of stimulated emission due to quantum cascade processes [10]. The strategy perhaps investigated most intensively considered the generation of collective Josephson oscillations by a lattice of moving Josephson vortices, exciting electromagnetic cavity resonances inside the stack, see e.g., [11–19]. Here, typically stacks with lateral dimensions of a few microns or smaller, consisting of some 10 junctions have been studied, perhaps with modest success. By contrast, in a recent experiment [20] much larger mesa structures consisting of almost 1000 junctions having lateral dimensions in the 100 μm range have been used to observe coherent off-chip THz radiation with an output power of some μW. Phase synchronization was presumably achieved via the excitation of cavity resonances. This experiment immediately triggered activities to understand the mechanism of THz generation in large intrinsic junction stacks [21–24]. Here we report on a study of such structures using low temperature scanning laser microscopy (LTSLM), cf. Fig. 1. In LTSLM a laser beam locally warms up a sample by a few K. The local change of temperature dependent electric quantities such as resistivity causes a global voltage response ΔV across the sample which serves as the contrast for a LTSLM image. This method allows for the visualization of electric field and current distributions with a lateral resolution of some μm. Standing electromagnetic waves have been imaged this way. Furthermore, the large structures used in [20]—even larger structures have been suggested [21]—are prone to

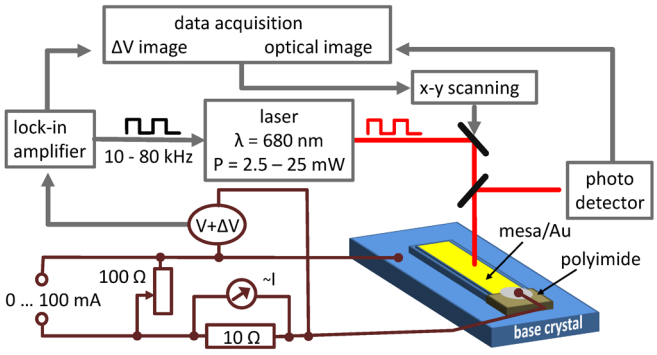

FIG. 1 (color online). Principle of low temperature scanning laser microscopy (LTSLM). The beam of a diode laser is deflected by a scanning unit and focused onto the sample surface (spot size 1–2 μm). In order to provide a load line for stable operation, the mesa covered with Au is biased using a current source and variable resistor parallel to the mesa. Local laser heating by a few K (affecting an in-plane area of a few μm and about half of the mesa thickness, cf. Fig. S1 in Ref. [31]), causes a response ΔV serving as the contrast for the LTSLM image. In order to improve the signal-to-noise ratio the beam is modulated at 10–80 kHz and ΔV is detected by a lock-in amplifier.

substantial heating. LTSLM is also able to shine light on such heating effects.

For the experiments BSCCO single crystals were grown using the floating zone technique, and annealed at 600 °C and 1 atm (Ar 99% and O_2 1%). A T_c of about 83 K is typical for our slightly underdoped samples. To provide good electrical contact the single crystals were cleaved in vacuum and a 60 nm Au layer was sputtered *in situ*. Then conventional photolithography was used to define the mesa size in the *a-b* plane (330 μm long and 30 to 80 μm wide). Ar ion milling yielded a mesa thickness of 1 μm along the *c* axis, with $\approx$670 intrinsic junctions in the stack. Insulating polyimide was used to surround the mesa edges, and an Au wire was attached to the mesa by silver paste. Other Au wires were connected to the big single crystal pedestal as grounds. In order to provide a load line for stable operation, the mesas were biased using a current source and variable resistor in parallel to the mesa, cf. Fig. 1. In total we measured 6 mesas on 3 different crystals.

We first discuss data of a 40 μm wide mesa. Figure 2 shows the current-voltage characteristic (IVC) at temperature $T = 25$ K together with LTSLM data, taken in a bias regime where THz emission was detected in [20]. A more complete set of LTSLM images is shown as Fig. S2 in Ref. [31]. For $V > 480$ mV the LTSLM images are smooth, cf. image *A*, except for an enhanced response ΔV along the mesa edge. Here, the laser warms up the mesa more effectively than in the inner region where it is attenuated by the gold layer covering the mesa surface. Note that in the warmed up regions all *T*-dependent parameters change; particularly the in-plane and out-of-plane critical supercurrent densities are reduced and the quasiparticle conductances are increased, leading to an increased damping both along and perpendicular to the layers. The negative sign of ΔV seen in image *A* is consistent with the fact that the *c*-axis (subgap) resistance of the junctions decreases with increasing *T*. At lower voltages, cf. images *B* and *C*, a wavelike structure appears which is very reminiscent of images of standing electromagnetic waves (cavity resonances), from low temperature scanning electron beam microscopy (LTSEM) both for conventional Josephson junctions [25,26] and intrinsic Josephson junction stacks [18]. LTSEM imaging of cavity modes excited in single Nb junctions has been analyzed in detail in Refs. [25,26]; the same physics holds for LTSLM. To gain a qualitative understanding we first note that a cavity mode excited in a junction leads to a step structure on the IVC, the shape and voltage position of which depends on its resonance frequency and its quality factor. The local increase in damping caused by the beam leads to a change ΔQ in the quality factor of the resonance which in turn changes the (global) voltage across the junction. For small relative changes $\Delta Q/Q$ one finds a linear response, $\Delta V \propto Q$ [25]. ΔQ depends on the position of the electron (or laser) beam. Let us assume that a 1D resonance with a *c*-axis electric field $\propto \cos(kx)$ is excited, where $x = 0$ denotes the edge of the junction. If the beam-induced change in the in-plane damping is the dominating effect (which is the case for Nb junctions) ΔV becomes proportional to $\sin^2(kx)$; if the change in out-of-plane damping dominates one finds $\Delta V \propto \cos^2(kx)$.

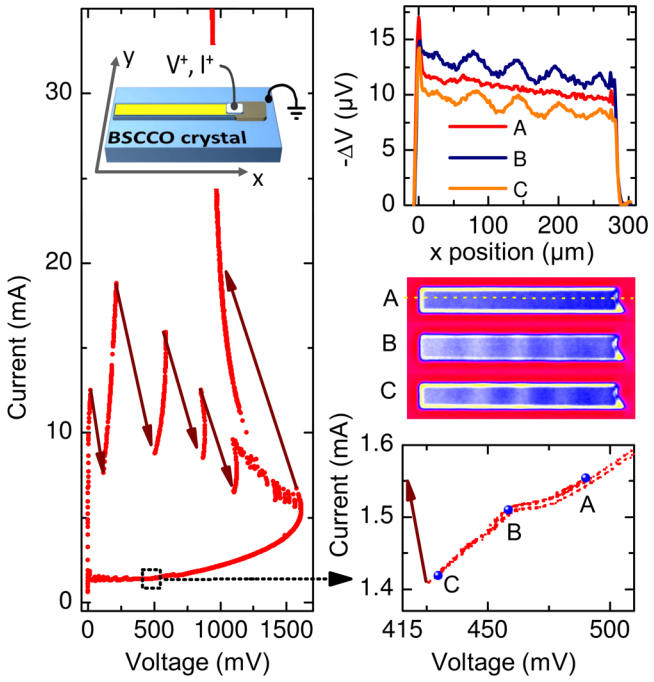

FIG. 2 (color online). 40×330 μm^2 BSCCO mesa, at $T = 25$ K. Left: current-voltage characteristic (IVC) on large current and voltage scales. Solid arrows denote jumps in the IVC; inset shows the geometry of the device. Right: enlargement of the IVC (bottom) in the region where LTSLM images (*A*–*C*; shown above) were recorded. Upper graph shows line scans from images *A*–*C*, along the long side of the mesa at half width, cf. dashed line in image *A*. For a more complete set of LTSLM images, see Fig. S2 in Ref. [31].

Thus the period in the LTSLM image equals half the wavelength λ ($\approx$120 μm in our case) of the cavity mode. Qualitatively, when the beam heats up a position where the relevant field component (magnetic or electric) has a node there is no effect on *Q*; the effect is maximum when the beam is at an antinode. For a BSCCO stack the same physics holds, with the additional feature that only collective resonances give a clear wavelike image. The LTSLM images of Fig. 2 were taken in a state where 60%–70% of all junctions were resistive while the others carried no dc voltage, as estimated from the ratio of the voltages on the branch investigated and the outermost branch. The average voltage per junction, say for image *D*, is 1–1.2 mV; using Josephson's relation we estimate $f \approx 0.5$–0.6 THz and find a mode velocity $c = f\lambda \approx (6$–$7) \times 10^7$ m/s, which is close to the highest possible value $c_0/n \approx 9 \times 10^7$ m/s, where c_0 is the vacuum speed of light and $n \approx 3.5$ is the far-infrared diffraction index [20]. Thus, the pattern imaged is consistent with the THz emission observed in [20], although in our case we see that the wave forms along the long side (in [20] the fundamental cavity mode with one

half wave along the short side seemed to have formed). We note that, as for the single Nb junction case [25,26], ΔV is negative and the wave structure seems to have a node at the junction edge. The effect of changes in in-plane damping thus seems to dominate the response. We further note that the images obtained did not depend on the scan direction (i.e., beam scanned along x or y direction). Also, at the mesa edges, where the crystal is not covered by Au and the absorbed laser power is higher, the signal is stronger but shows the same features as the interior of the mesa. We can thus state that these features are *detected* but not *created* by the laser beam. For this mesa we have seen similar patterns on several branches on the IVC (i.e., with different numbers of junctions in the resistive state). However, for the other mesas we could not find corresponding signals. These kinds of cavity modes seem to be difficult to excite.

We next focus on higher bias currents I. Figure 3 shows data for a 30 μm wide mesa. At $I < 16$ mA the LTSLM images, apart from edge signals, show a broad response being strongest near the contact lead (cf. image A) and the corresponding line scan. Slightly above 16 mA two bright stripes appear right of the current lead, cf. image B. With further increasing I these two stripes move away from each other until, above 22 mA, cf. image E, the right stripe joins the edge signal while the left stripe continues to move towards the left mesa edge. The feature seen here is very indicative of a hot spot, as observed for superconducting thin film bridges. In such bridges, a certain area is driven to above T_c in the case of a large dc input power and is self-sustained due to Joule heating [27]. For conventional superconducting thin films with in-plane current flow such hot spots have been imaged by LTSEM [28,29]. In these LTSEM experiments, when the beam touches the edge of the hot spot it increases its size, leading to a signal $\Delta V > 0$. By contrast, both in the "hot" and in the "cold" regions no drastic change occurs and $\Delta V \approx 0$. Note that in our case the input power of ≈ 10 mW brings the mesa temperature close to T_c even before hot spot formation sets in. For the mesas studied here, both in-plane and out-of-plane currents may contribute to such a hot spot formation due to nonuniformity of current flow, at least near the contacts where current is injected and the hot spot feature appears first. The in-plane dissipation, which steeply increases with T at T_c, should result in an effect basically identical to the conventional hot spot case. By contrast, the c-axis resistance decreases (smoothly) with increasing T (through T_c). Hence, the sign of the overall voltage response upon hot spot formation is hard to judge. However, we still expect the signal to be strongest at the edge of the hot spot, qualitatively leading to the same images of beam-induced voltage [30]. Note that the IVC shows a small jump towards lower voltages at $I \approx 16$ mA when the hot spot feature appears first. Thus, the global voltage response upon hot spot formation is *negative*, which clearly indicates that the c-axis contribution to the voltage response upon hot spot formation dominates over the in-plane contribution and which may also explain the negative sign of the laser-induced ΔV. Still, the fact that we observe hot spot nucleation at the current contact indicates that the inhomogeneous in-plane current contribution might trigger and perhaps stabilize the hot spot. For mesas of larger width the hot spot feature becomes elliptic in shape, cf. Fig. S2 in Ref. [31] for a 70 μm wide mesa.

At $I \approx 23$ mA, cf. images C–E, wavelike structures appear left of the hot spot boundary. Three maxima can be seen. The distance between them is 55 μm. Interpreting the structures as a standing electromagnetic wave we associate a wavelength of $\lambda \approx 110$ μm with it. The frequency of this mode can be estimated from the total voltage drop across the mesa, $V = 610$ mV, yielding

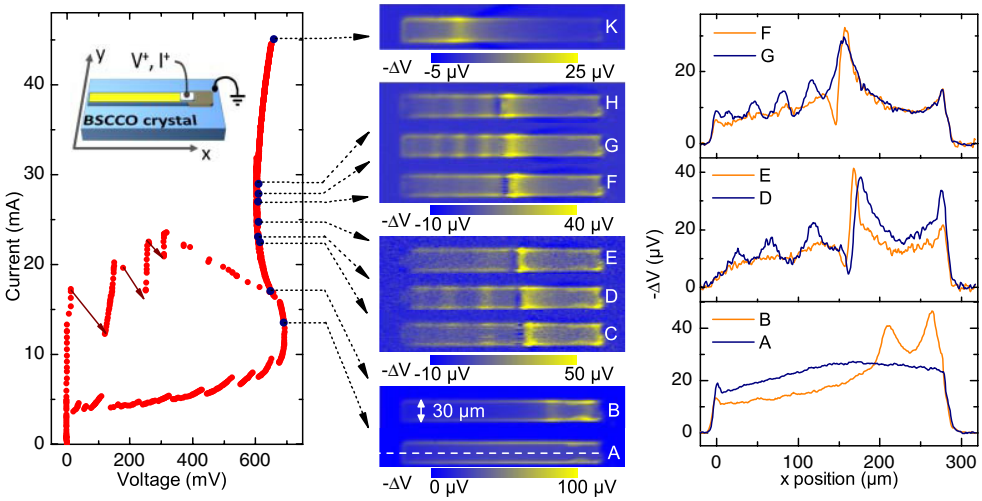

FIG. 3 (color online). Current-voltage characteristic and LTSLM data of a 30×330 μm^2 large BSCCO mesa at 50 K. Red solid arrows in the IVC denote switching processes, black arrows indicate bias points where LTSLM images A–K have been taken. Displayed on the right are line scans from images A, B, D–G along the long side of the mesa at half width, cf. white dashed line in image A.

$f \approx 0.44$ THz and a mode velocity of 4.8×10^7 m/s, which is about a factor of 2 lower than c_0/n. With increasing I the wave feature first disappears, but, near 28 mA, is replaced by another wavelike feature exhibiting 4 maxima at a distance of 35 μm, cf. image G. The corresponding wavelength is $\lambda \approx 70$ μm and the calculated mode velocity is 3×10^7 m/s. We also found standing-wave patterns for wider mesa structures, cf. Fig. S3 in Ref. [31] for a 70 μm wide mesa. We also note that in the high bias region we saw hot spots without wave features but never wave features without a hot spot. For an N junction stack there are N different mode velocities c_q [11,12,32], the fastest of which decreases inversely proportional to the mode index q counting the number of half waves perpendicular to the layers. Thus, modes with, respectively, $q = 2$ and 3 may have been excited. However, one should also consider a mode velocity c_1 which is lower than c_0/n. Such a scenario is realistic, since even the ''cold'' part of the mesa is likely to have a temperature not too far from T_c. In that case, the in-plane London penetration depth $\lambda_\parallel$ can become comparable to the mesa thickness d and, as discussed in Ref. [31], the in-phase mode velocity becomes $c_1 \approx 0.13(c_0/n) \times (d/\lambda_\parallel)$, approaching zero for $T \to T_c$. For $\lambda_\parallel \approx 0.5$ μm (88% of T_c for BSCCO) one obtains $c_1 \approx 3 \times 10^7$ m/s in agreement with the mode velocity of the resonance near 28 mA.

Having interpreted the wave structure in terms of an electromagnetic wave (without having measured THz emission directly) we should also discuss alternative explanations. In the 70 μm wide mesa of Fig. S3 [31] the wave structure appeared in a region of negative differential resistance. One could assume that, like in a Gunn diode, some domains move along the junctions giving rise to the observed pattern. However, for the case of the 30 μm wide mesa shown in Fig. 3 the differential resistance was positive in the regime where the wave structures appear, making this explanation unlikely. Further, the resonances appeared only at bath temperatures well below T_c, and a magnetic field of about 60 G applied parallel to the layers, was sufficient to destroy the pattern, cf. Fig. S4 in Ref. [31]. All this strongly points to an interpretation in terms of the Josephson effect. Regarding the role of the hot spot we note that its edge is typically a half wavelength away from the first antinode of the wave. The hot spot seems to have an active role in the formation of the standing wave. The most likely explanation is that the edge of the hot spot may be viewed as a resistive termination of the cavity formed by the cold part of the junction which is adjustable in space by applying variable values of bias current. It thus, in a natural way, combines the approaches of shunting intrinsic junctions and using internal cavity resonances to synchronize the different junctions in the stack. The effect may serve as an important tool to tune synchronous THz emission from intrinsic Josephson junction stacks.

We gratefully acknowledge financial support by the Strategic Japanese-German International Cooperative Program from the JST & DFG and by INTAS Grant No. 05-1000008-7972.

[1] B. Ferguson and X. C. Zhang, Nature Mater. **1**, 26 (2002).
[2] R. Kleiner *et al.*, Phys. Rev. Lett. **68**, 2394 (1992).
[3] A. A. Yurgens, Supercond. Sci. Technol. **13**, R85 (2000).
[4] I. Batov *et al.*, Appl. Phys. Lett. **88**, 262504 (2006).
[5] H. B. Wang *et al.*, Appl. Phys. Lett. **77**, 1017 (2000).
[6] A. Grib *et al.*, Supercond. Sci. Technol. **19**, S200 (2006).
[7] S. Madsen, G. Filatrella, and N. F. Pedersen, Eur. Phys. J. B **40**, 209 (2004).
[8] K. Lee *et al.*, Phys. Rev. B **61**, 3616 (2000).
[9] E. Kume, I. Iguchi, and H. Takahashi, Appl. Phys. Lett. **75**, 2809 (1999).
[10] V. M. Krasnov, Phys. Rev. Lett. **97**, 257003 (2006).
[11] R. Kleiner, Phys. Rev. B **50**, 6919 (1994).
[12] R. Kleiner, T. Gaber, and G. Hechtfischer, Phys. Rev. B **62**, 4086 (2000).
[13] A. V. Ustinov and S. Sakai, Appl. Phys. Lett. **73**, 686 (1998).
[14] M. Machida *et al.*, Physica C (Amsterdam) **330**, 85 (2000).
[15] S. Heim *et al.*, Supercond. Sci. Technol. **15**, 1226 (2002).
[16] H. Fujino *et al.*, Physica C (Amsterdam) **367**, 404 (2002).
[17] M. H. Bae, H.-J. Lee, and J.-H. Choi, Phys. Rev. Lett. **98**, 027002 (2007).
[18] T. Clauss *et al.*, Appl. Phys. Lett. **85**, 3166 (2004).
[19] H. B. Wang *et al.*, Appl. Phys. Lett. **89**, 252506 (2006).
[20] L. Ozyuzer *et al.*, Science **318**, 1291 (2007).
[21] L. N. Bulaevskii and A. E. Koshelev, Phys. Rev. Lett. **99**, 057002 (2007).
[22] A. E. Koshelev and L. N. Bulaevskii, Phys. Rev. B **77**, 014530 (2008).
[23] A. E. Koshelev, Phys. Rev. B **78**, 174509 (2008).
[24] S. Lin and X. Hu, Phys. Rev. Lett. **100**, 247006 (2008).
[25] B. Mayer *et al.*, Phys. Rev. B **44**, 12463 (1991).
[26] S. G. Lachenmann *et al.*, Phys. Rev. B **48**, 3295 (1993).
[27] W. J. Skocpol, M. R. Beasley, and M. Tinkham, J. Appl. Phys. **45**, 4054 (1974).
[28] R. Eichele *et al.*, J. Low Temp. Phys. **52**, 449 (1983).
[29] D. Doenitz *et al.*, Appl. Phys. Lett. **90**, 252512 (2007).
[30] One should also consider the possibility that in the ''hot'' region the temperature is still below T_c but one faces a suppressed gap due to heavy quasiparticle injection; see R. Gross, B. Schmid, and R. P. Huebener, J. Low Temp. Phys. **62**, 245 (1986) and references therein. However, when we keep increasing the dc power in our stack after the hot spot feature has formed we do not see any other transition (say, to a ''real'' hot spot or to a state where the gap takes another nonequilibrium value). We thus do not think that this effect is active here.
[31] See EPAPS Document No. E-PRLTAO-102-055902 for details of LTSLM, additional transport and LTSLM data and an estimate of the in-phase mode velocity for large junction numbers and temperatures close to T_c. For more information on EPAPS, see http://www.aip.org/pubservs/epaps.html.
[32] R. Kleiner, T. Gaber, and G. Hechtfischer, Physica C (Amsterdam) **362**, 29 (2001).